# Scalable Synthesis of Defect Abundant Si Nanorods for High-Performance Li-Ion Battery Anodes

**Jing Wang,*,† Xiangcai Meng,† Xiulin Fan,‡ Wenbo Zhang,† Hongyong Zhang,† and Chunsheng Wang*,‡**

†School of Materials Science and Engineering, Jiamusi University, Jiamusi 154007, China and ‡Department of Chemical and Biomolecular Engineering, University of Maryland, College Park, Maryland 20742, United States

**ABSTRACT** Microsized nanostructured silicon–carbon composite is a promising anode material for high energy Li-ion batteries. However, large-scale synthesis of high-performance nano-Si materials at a low cost still remains a significant challenge. We report a scalable low cost method to synthesize Al/Na-doped and defect-abundant Si nanorods that have excellent electrochemical performance with high first-cycle Coulombic efficiency (90%). The unique Si nanorods are synthesized by acid etching the refined and rapidly solidified eutectic Al–Si ingot. To maintain the high electronic conductivity, a thin layer of carbon is then coated on the Si nanorods by carbonization of self-polymerized polydopamine (PDA) at 800 °C. The carbon coated Si nanorods (Si@C) electrode at 0.9 mg $cm^{-2}$ loading (corresponding to area-specific-capacity of ~2.0 mAh $cm^{-2}$) exhibits a reversible capacity of ~2200 mAh $g^{-1}$ at 100 mA $g^{-1}$ current, and maintains ~700 mAh $g^{-1}$ over 1000 cycles at 1000 mA $g^{-1}$ with a capacity decay rate of 0.02% per cycle. High Coulombic efficiencies of 87% in the first cycle and ~99.7% after 5 cycles are achieved due to the formation of an artificial $Al_2O_3$ solid electrolyte interphase (SEI) on the Si surface, and the low surface area (31 $m^2$ $g^{-1}$), which has never been reported before for nano-Si anodes. The excellent electrochemical performance results from the massive defects (twins, stacking faults, dislocations) and Al/Na doping in Si nanorods induced by rapid solidification and Na salt modifications; this greatly enhances the robustness of Si from the volume changes and alleviates the mechanical stress/strain of the Si nanorods during the lithium insertion/extraction process. Introducing massive defects and Al/Na doping in eutectic Si nanorods for Li-ion battery anodes is unexplored territory. We venture this uncharted territory to commercialize this nanostructured Si anode for the next generation of Li-ion batteries.

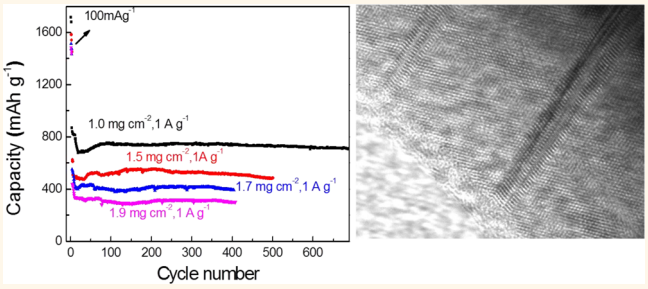


**KEYWORDS:** lithium-ion battery · silicon anode · eutectic Al–Si ingot · PDA self-polymerization

The ever-growing demands for high-performance power sources, especially in electrical vehicles (EV) and large-scale renewable energy storage units, have stimulated tremendous research interest toward developing the next generation of Li-ion batteries (LIBs) with high energy density, long cycle life, and low cost.[1−3] Today's commercial graphite anode can provide capacity of 350 mAh $g^{-1}$, which has been very close to the theoretical value (372 mAh $g^{-1}$),[4] and alternative high capacity anodes have to be explored. Silicon (Si) has a 10 times higher theoretic specific capacity (3579 mAh $g^{-1}$) than graphite[5,6] and has been regarded as the most promising candidate for next-generation LIBs. However, bulk Si anodes suffer from poor cycle life and low Coulombic efficiency due to the large volume change (~300%) during the lithiation/delithiation process.[5] Moreover, the low electronic conductivity of silicon ($6.7 \times 10^{-4}$ S/cm)[7] also reduces the power density.

Tremendous efforts have been made in recent years to improve the performance of Si anodes by using nanoporous Si, where the pores can effectively accommodate the large volume expansion during lithiation/delithaition. Various nanoporous Si materials such as nanotubes, hollow spheres and core–shell structures[8−11] were designed for Li-ion battery anodes. The pomegranate-like Si–C yolk–shell structures[12] show stable areal capacity of 1.2 mAh $cm^{-2}$ over 200 cycles. However, scalable synthesis of

* Address correspondence to jmsdxwangjing@163.com, Email:cswang@umd.edu.

Received for review April 28, 2015 and accepted May 26, 2015.

**Published online May 26, 2015**
**10.1021/acsnano.5b02565**

such a high-performance nanoporous Si material at a low cost remains a significant challenge. Although significant advances have been achieved for nanostrcured Si anodes in recent years, nano-Si anode materials still have not been commercialized yet for Li-ion batteries due to either unsatisfactory performance, scale-up capability, or high cost.

Recently, scalable chemical etching method has been applied to synthesize porous Si[12−14] and solid Si nanorods[15] for Li-ion battery anodes. Although the porous Si can provide a stable capacity of >750 mAh $g^{-1}$ over 1000 cycles and high power density,[2,14] the large surface area of porous Si significantly reduces the first-cycle Coulombic efficiency because of the formation of large amounts of solid electrolyte interphase (SEI), thus limiting them for practical Li-ion battery applications. In contrast, micro-sized solid Si nanorods with a small surface area synthesized from scalable chemical etching have high first-cycle Coulombic efficiency, but suffer from poor cycle life due to the formation of cracks induced by large volume changes in the lithiation/delithiation.[15] The large volume change (>300%) during the lithiation generates very high stress and defects in Si nanorods, resulting in cracks due to the brittleness nature and anisotropic crystal structure of Si nanorods.[16−18] However, recent research demonstrates that with further lithiation, the accumulation of defects in the lithiation of Si changes the brittle Si into plastic $Li_xSi$, resulting in a plastic flow at the late stage of lithiation.[19−22] The plastic flow releases the stress, thus avoiding formation of cracks during further lithiation. If we can pregenerate a large number of defects (but crack-free) in Si nanorods, the flow stress may be significantly reduced to allow the plastic flow of Si nanorods before cracking; thus, the cracks can be reduced or even avoided during lithiation/delithaion cycles. Therefore, the existing defects such as dislocations, twins, and stacking faults in Si may significantly enhance the cycle life of Si nanorods. The challenge is how to synthesize the Si nanorods with a large number of pre-existing defects, but without cracks using a scalable low-cost method.

In this study, we synthesize Al/Na doped Si nanorods (<200 nm in diameter and 5−20 $\mu$m in length) containing large number of defects (but crack-free) by simply etching the eutectic Al−Si ingot that is rapidly solidified in a water circulated Cu mold after adding 3% Na modifiers. The modifications with modifiers and rapid solidification are to (1) generate a large number of defects (twins, stacking faults, dislocations), (2) change the morphology of eutectic Si from plate to nanorods, and (3) increase the level of Al and Na doping in Si. The surface Al and Si will be oxidized in air into $Al_2O_3$ and $SiO_x$ to function as an artificial SEI, improving the Coulombic efficiency.[23] Different from interconnected dendrite Si obtained from etching of the commercial eutectic Al−Si spheres that can only maintain capacity of 1800 mAh $g^{-1}$ for 70 cycles[24] or 1500 mAh $g^{-1}$ over 190 cycles[25] with a very low first-cycle Coulombic efficiency of 40%−70%, the eutectic Si nanorods in this study from the modified and quenched eutectic Al−Si ingot have massive defects (twins, stacking faults, and dislocations) and have extremely high first-cycle Coulombic efficiency of >87% and maintain ~600 mAh $g^{-1}$ at 300 mA $g^{-1}$ for 200 cycles. After carbon coating, the defect abundant Si@C nanorods at loadings of 0.9−1.9 mg $cm^{-2}$ can provide 1500−2200 mAh $g^{-1}$ at 100 mA $g^{-1}$ with the first-cycle Coulombic efficiencies of 84−87%. The Si@C anodes with loading 0.9 mg $cm^{-2}$ can maintain ~700 mAh $g^{-1}$ at 1000 mA $g^{-1}$ for over 1000 cycles. The cycle stability (0.02% capacity decay per cycle) and first-cycle Coulombic efficiency (~87%) is among the best performances of silicon anodes synthesized using the scalable method reported to date. These promising results suggest that Al/Na doped and defect abundant Si nanorods synthesized using etching Al−Si ingot, which has been widely used in foundry industry to enhance the tensile elongation of eutectic Al−Si alloys,[26] can potentially be commercialized for high energy Li-ion batteries.

## RESULT AND DISCUSSION

**Synthesis and Characterization.** The preparation procedures for the Si nanorods and carbon coating are illustrated in Figure 1. Typically, the eutectic Al−13% Si ingots were prepared by melting Al−Si intermediate alloys at a designed composition at 760 °C in an induction furnace, and then quenched in water circulated copper molds after adding 3% Na modifiers. The Si nanorods were obtained after etching Al using an 8% HCl solution, filtering, water washing, and drying in a vacuum at 80 °C. To improve Si conductivity, a thin layer of carbon was coated on Si by *in situ* self-polymerization of DA to form PDA anchored on Si surfaces and then carbonization at 800 °C. The purpose of modification and rapid solidification is to reduce the size of Si nanorods, generate more defects, and dissolve more Al in Si nanorods.

X-ray Diffraction (XRD) patterns of the eutectic Al−13% Si ingots, etched eutectic Si, and carbon coated eutectic Si (Si@C) are shown in Supporting Information Figure S1a. All XRD peaks of the quenched eutectic Al−13% Si ingot can well be indexed to the Si (JCPDS No. 99-0092) and Al (JCPDS No. 04-0787). After HCl etching Al under vigorous stirring overnight, the peaks at 28.70°, 47.50°, 56.30°, 69.3°, and 78° can be indexed to the (111), (220), (311), (400), and (331) of crystal Si, and Al peaks are almost invisible. After carbon coating, very weak dispersion-peaks at around 28°, 42°, and 62° are ascribed to partially amorphous carbon for Si@C sample. The morphology of quenched eutectic Al−13% Si ingots, etched eutectic Si was characterized using Scanning Electron Microscopy

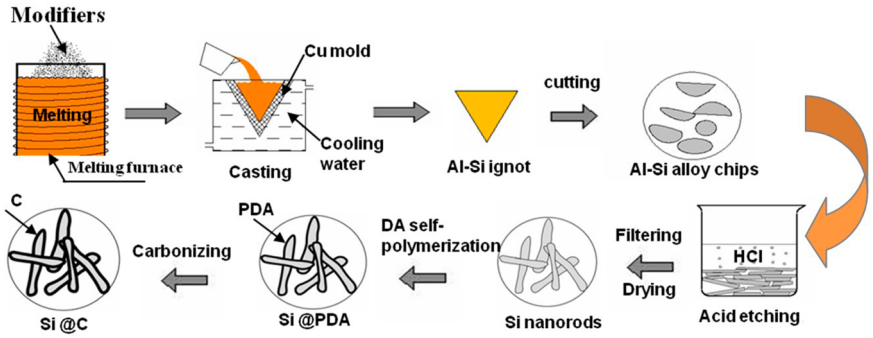


**Figure 1. Schematic illustration of synthesis procedure for carbon coated Si nanorods.**

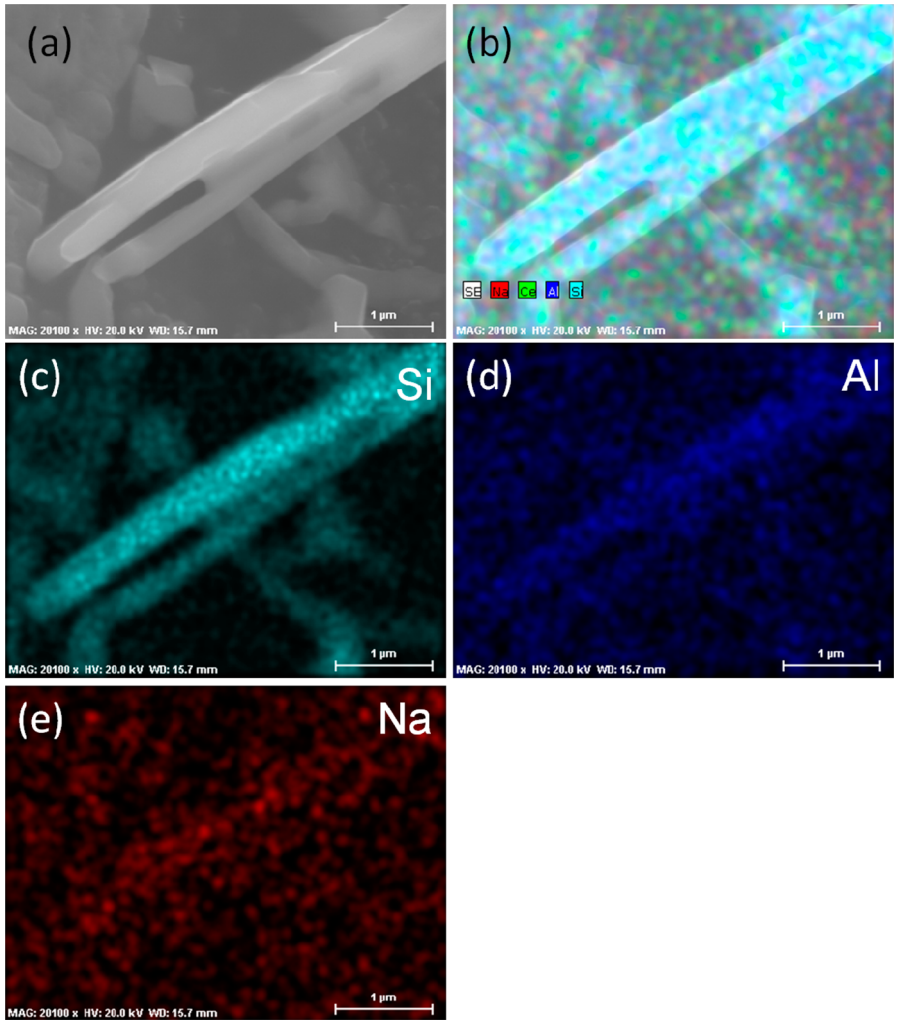


**Figure 2. SEM image of Si nanorods (a), and corresponding EDS elemental mapping images (b); Si mapping in cyan (c), Al mapping in blue (d); Na mapping in red (e).**

(SEM) and the corresponding elemental mapping was detected using Energy Dispersive X-ray Spectroscopy (EDS). As shown in Supporting Information Figure S1b, the quenched eutectic 2D-Si with 5−20 $\mu$m in length and 200 nm in thickness is uniformly dispersed in Al substrate. After HCl etching, 3D-Si has nanorod morphology (Supporting Information Figure S1c and Figure 2a) with the similar size as observed in Al−Si alloys (Supporting Information Figure S1b). The overlap of EDS mapping for Al and Si in modified and quenched Si nanorods (Supporting Information Figure S1d,e and Figure 2b−d) reveals that Al is dissolved in the Si since the Al mapping still did not change even after the vigorous stirring in 8% HCl overnight and repeat washing using distilled water. It was reported that up to ~5% Al can be dissolved in eutectic Si in the commercial Al−Si alloy under a low solidification rate;[24,27] the Al content in Si will be more

in quenched eutectic Al−Si alloys due to the rapid solidification. The surfaces of Si and Al are oxidized into $Al_2O_3$ and $SiO_x$ since the oxygen mapping overlaps with Si and Al (Supporting Information Figure S1f). The 2 nm $Al_2O_3$ and $SiO_x$ surface layer can be observed in high-resolution transmission electron microscope (HRTEM) images in Supporting Information Figure S1g. The surface $Al_2O_3$ and $SiO_x$ can function as an artificial solid electrolyte interphase (SEI), increasing the Coulombic efficiency (stabilizing SEI), thus improving the lithiation/delithiation cycle life.

In addition to Al (Figure 2d), Na is also doped into Si (Figure 2e) to change the nucleation and growth of the eutectic Si as a modifier. Na cannot alloy with Si since the first-principles calculations showed that the Si−Na phase has negative heats of formation. However, after doping with a small percentage of Al, Na can alloy with Si.[28] The Al and Na doping into Si can enhance the conductivity of silicon, increase the lattice size,[24] and reduce the volume expansion upon Li insertion and extraction, thus improving the cycle stability and rate performance.[29,30] In addition to Al and Na doping, a large number of defects are also generated in the eutectic Si due to modification and rapid solidification as demonstrated in HRTEM in Figure 3. The highly concentrated defects extending along the growth direction to the growth terminal exist in Si nanorods (Figure 3a, Figure S2 in Supporting Information). Planar defects such as stacking faults (Figure 3b) and micro-twin defects (Figure 3c) can be observed in the Si nanorods. The selected area electron diffraction (SAED) patterns (inset in Figure 3a) also confirmed the appearance of the micro-twin defects. The measured spacing of the lattice plane is 0.31 nm, which matches well with the (111) plane of the cubic diamond structure of Si (0.314 nm) (Figure 3b,d). It is much easier for (111) plane of Si crystal to emerge planar defects such as twin because of the low stacking fault energy. The stacking faults in Figure 3b are indicated as parallel dark lines. In addition, the planar spacing of stacking faults and the adjacent atomic layer have a little change, resulting in lattice distortion in Si crystals. Stacking faults are always associated with partial dislocations, which can emerge in the junction or transition zones between the stacking faults region and the complete crystal area. A lot of twin defects in Si nanorods consisting of few layers of atoms can be observed as micro-twins (Figure 3c). The modification and fast solidification induced defects in eutectic Si have been extensively investigated in the foundry committee. In the eutectic growth of Al−Si alloy, Si crystal is the leading phase, and α-Al nucleates and grows attaching eutectic Si. Unmodified crystal Si grows along the sole ⟨112⟩ crystal orientation with two crystal plane (111) concave angle twin through the twin plane reentrant edge mechanism. The two-dimensional growth steps allow continuous Si atoms "in-plane growth" of the (111) plane. Since the twin density of unmodified eutectic Si is quite low, and the branching course is limited, the unmodified eutectic Si grows radially with straight and thick plate-like morphology (Figure S3 in Supporting Information). After adding Na modifiers and solidification at a fast rate, large amount of twins and stacking faults (up to $10^5$ times) will be generated in eutectic Si.[31] The Na modifiers increase the twin density through impurity induced twinning mechanism, in which the modification elements adsorb on the Si surface and subsequently embed into Si lattice, which is liable to the production of stacking faults and then twins. Therefore, the Na modifier is rich in the eutectic Si as demonstrated in Figure 2e. The absorbed Na modifiers in Si change the growth pattern of eutectic Si from the anisotropy "in-plane growth" of the (111) plane to isotropy "out-of-plane growth", resulting in the morphology to transform from the thick-plates (Supporting Information Figure S3) to fibrous nanorods (Figure 2, Supporting Information Figure S1c).[32] Fast solidification has the same refined effect as the modifiers.[31] Under rapid solidification, the diffusion of expelled Si from Al is limited, resulting in a high Si concentration and composition undercooling in the front of the Si−liquid interfaces, thus increasing twin branching density. Eventually, as combined effects of modification and rapid solidification, microsized Si nanorods with massive defects (Figure 3) are formed in eutectics of Al−Si ingots. The large amount of pre-existing defects in Si nanorods can greatly reduce the flow stress and increase Li-ion diffusion kinetics in Si nanorods. The pre-existing defects could release the stress/strain through plastic deformation, thus leveraging the formation of cracking.

In addition to generation of the defects, the modification and rapid solidification are also favorable to form isotropic eutectic Si. Under addition of modifiers and rapid solidification, the growth of eutectic Si changes from the anisotropy "in-plane growth" to isotropy "out-of-plane growth", which may favor for isotropic lithiation, reducing the stress/strain and cracking. The modified and quenched Si nanorods are better than the oriented CVD Si nanowires that experience anisotropy lithiation due to the different lithiation rate in each orthogonal radial direction.[33]

To improve the electronic conductivity, a dense carbon layer was coated on eutectic Si nanorods using dopamine as a carbon source due to the high carbonization yield (60%) and its strong and versatile anchoring capability on Si.[34] Dopamine is employed to self-polymerize into polydopamine (PDA) films immobilized on Si surfaces with a robust adhesion; thus, complete and homogeneous carbon coatings with intimate bonding with Si can be formed after carbonization. Figure 3d shows that a 10 nm carbon layer is uniformly coated on the Si nanorods. Thermal gravity

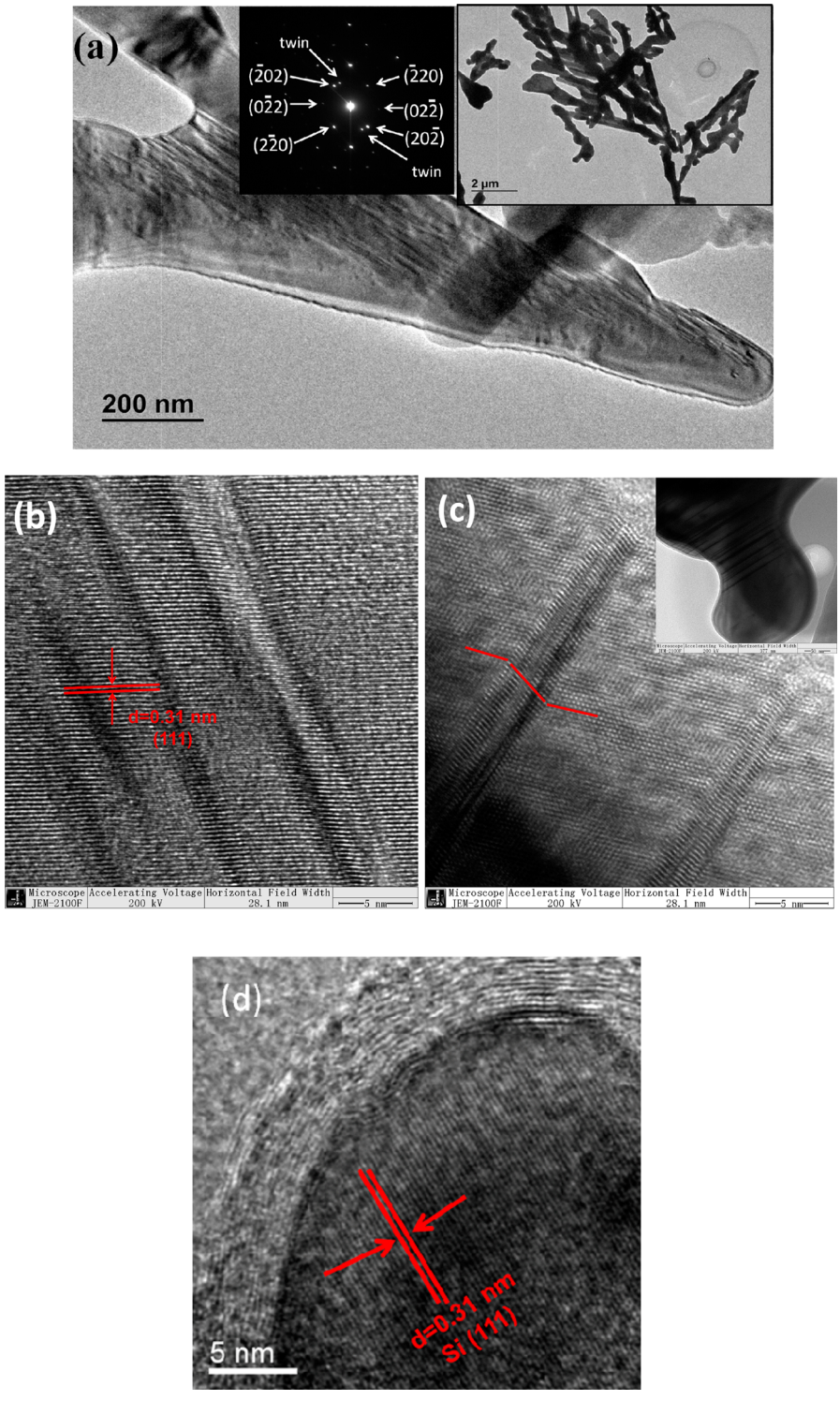


**Figure 3. TEM, corresponding SAED pattern and HRTEM images of eutectic Si nanorods and Si@C. (a) TEM image and SAED pattern of eutectic silicon, (b) HRTEM image of stacking faults, (c) HRTEM of micro-twin (the inset is the lower magnification image of the Si nanorod), (d) HRTEM image of eutectic silicon nanorods with 8−10 nm of carbon coating.**

analysis (TGA) measurement shows that the content of coated carbon is 16.5% (Supporting Information Figure S4). The degree of graphitization of coated carbon on Si nanorods was characterized using Raman spectroscopy. The Raman of uncoated Si nanorods and Si/C (PVDF as carbon source) were also used as a control (Supporting Information Figure S5). In the Si nanorod sample, the sharp peak at 517 $cm^{-1}$ and weak peaks at 297 and 931 $cm^{-1}$ are attributed to Raman vibration peaks of crystalline Si.[35,36] The three peaks are still clearly visible in Si/C composite. However, in Si@C nanorods, the peak intensity at 517 $cm^{-1}$

significantly decreases and the peaks at 297 and 931 $cm^{-1}$ almost disappear, demonstrating the formation of conformal carbon coating on Si nanorods. The two high vibration peaks at 1335 and 1590 $cm^{-1}$ for Si@C nanorods belong to carbon Raman vibration mode. The peak at 1335 $cm^{-1}$ reflects the vibration mode of noncrystal graphite (D band); the other peak at 1590 $cm^{-1}$ (G band) represents $E_{2g}$ vibration mode of crystal graphite.[37] The ratio of intensity of D and G peaks ($I_D/I_G$ = 1.04) reflects the low degree of graphitization of coated carbon, which is in accordance with XRD results of amorphous carbon (Supporting Information Figure S1a). The bonding between coated carbon and Si nanorods was also characterized using Fourier transform infrared (FTIR) spectroscopy (Supporting Information Figure S6). The FTIRs of Si nanorods and Si/C composites were also shown in Figure S6 for comparison. The bands at 1060, 1380, 1620, and 3430 $cm^{-1}$ corresponding to the characteristic vibrations of the function groups on Si nanorods become weak and broaden in Si@C. Notably, the band at 1060 $cm^{-1}$ is splitted into the two peaks at 1240 and 1090 $cm^{-1}$ in Si@C nanorodes, while this 1060 $cm^{-1}$ band still maintains unchanged for the sample of Si/C composite. This result provides concrete proof for the formation of robust bonding on the interfaces between Si nanorods and coated carbon. The strong bonding between carbon and Si will improve cycle stability and stabilize the SEI and enhance the Coulumbic efficiency during the charge/discharge cycles.[38] Since the first cycle Coulombic efficiency is mainly controlled by the surface area, the Brunauer–Emmett–Teller (BET) specific surface area and pore size distribution were analyzed using nitrogen absorption measurements (Supporting Information Figure S7). The flat sorption isotherms from 0.2 to 0.8 show the existence of a small number of mesopores in both Si and Si@C (Figure S7a). However, due to the long nanorod size (5–20 $\mu$m), the BET surface area of the Si nanorods is only 12.96 $m^2\ g^{-1}$ and narrow pore distribution centers at 2–10 nm (Figure S7b). Therefore, increase of nanorod length is sufficient to reduce the specific surface area. The surface area of modified and quenched eutectic Si nanorods is over 1 order of magnitude less than that of all the reported nanostructured Si using the scalable method. For example, it is 10 times less than that of unmodified eutectic Si [102–103 $m^2\ g^{-1}$][24,25] and 40 times less than porous Si [495 $m^2\ cm^{-1}$] using HF etching[2] and 30 times less than that of porous Si synthesized using Mg reduction of $SiO_2$ [323 $m^2\ cm^{-1}$].[14] After carbon coating on Si surfaces, the BET surface of Si@C slightly increases to 30.98 $m^2\ g^{-1}$ with a pore size of 3.65 nm, but the value of 30.98 $m^2\ g^{-1}$ is still 5–10 times less than that reported for nano-Si. The low BET surface of Si@C demonstrates that coated carbon is relatively dense. The low surface area and formation of artificial $Al_2O_3$ SEI will greatly reduce the first cycle irreversible capacity, thus increasing the initial Coulombic efficiency.

**Electrochemical Performance.** Figures 4a,b show the first two charge–discharge curves of the Si@C and Si nanorods with the same loading of 0.9 mg $cm^{-2}$ at charge/discharge current of 100 mA $g^{-1}$. The specific capacity value reported in this work is based on the total weight of Si and graphite (Si80G20) after subtracting the 200 mAh $g^{-1}$ capacity of carbon black (15%). As shown in Figure 4a,b, the first discharge potential of Si rapidly drops to 0.1 V and enters into a long and flat voltage platform, corresponding to the Li-insertion process of crystalline Si to form an amorphous $Li_xSi$ phase,[39] providing a lithation capacity of 2529 mAh $g^{-1}$ for Si@C and 2502 mAh $g^{-1}$ for Si. The first delithiation curves present a voltage platform at about 0.4 V, similar to delithium intercalation behavior of amorphous silicon,[40] with the first charging capacity of 2200 mAh $g^{-1}$ for Si@C and 2239 mAh $g^{-1}$ for Si. The striking difference from the reported nano-Si is that the SEI formation plateau at 0.8 V is almost invisible in the first lithiation curves of both Si and Si@C anodes, demonstrating that only a very small amount of SEI is formed. It is also confirmed by the very high first cycle Coulombic efficiency of ~90% for Si and ~87% for Si@C (Figure 4a,b), which is among the highest in all reported nanostructured Si anodes synthesized using the scalable method[2,13,14,24,25] due to the low surface area and spontaneously formed artificial $Al_2O_3$ SEI. The slightly lower first-cycle Coulombic efficiency of Si@C than that of Si is due to the 3 times larger surface area of Si@C. In the second lithiation, a slope discharge curve is observed due to the lithiation of amorphous silicon,[41] and the delithiation curves are almost identical to the first delithiation, demonstrating excellent stability. Also, after the first cycle, the Coulombic efficiency for Si@C shows a value higher than 95% in the second cycle and nearly 99% in the third cycle (inset in Figure 4c). To confirm the high first cycle Coulombic efficiency and robust cycling stability of Si@C, several batches of Si@C materials were used to fabricate the anodes with loading varying from 1.0 to 1.9 mg $cm^{-2}$. The first cycle Coulombic efficiencies of all Si@C anodes are in a range of 84–88% (inset in Figure 4d), which is just slightly lower than the commercial graphite anodes. Since the high-performance Si nanorods were synthesized using the cheap scalable method, Si@C has a high potential for practical Li-ion battery application.

In addition to the high first cycle Coulombic efficiency, Si nanorods and the carbon coated Si nanorods also show long cycling stability. After charging/discharging at 100 mA $g^{-1}$ for two cycles, the current was increased to a high current of 1000 mA $g^{-1}$ for Si@C and 300 mA $g^{-1}$ for Si to test the long-term cycling stability. Figure 4c shows the representative capacity stability of Si and Si@C anodes. The Si nanorods show a

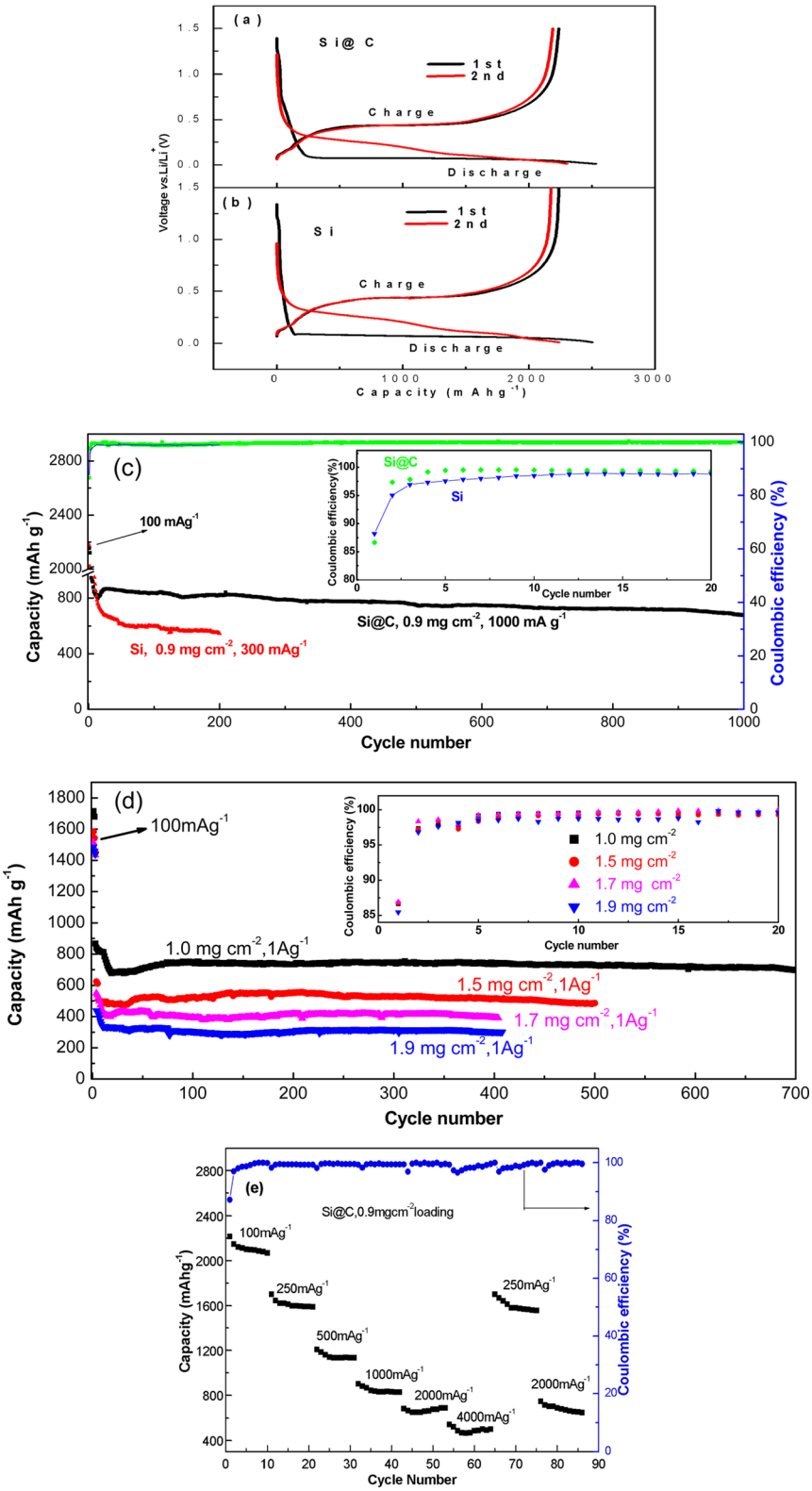


**Figure 4. First two discharge/charge behaviors of (a) Si@C anode, and (b) Si anode, (c) capacity stability of the Si@C and Si anodes at loading of 0.9 mg cm$^{-2}$, (d) the capacity stability of Si@C at a different loadings, and (e) rate capability behaviors of the Si@C composite electrode at current density from 100 to 4000 mA g$^{-1}$.**

stable capacity of 600 mAh g$^{-1}$ at 300 mA g$^{-1}$ over 200 cycles. The Si@C provides high capacity of ~700 mAh g$^{-1}$ even at 1000 mA g$^{-1}$ and retains ~80% of the 20th cycle capacity (850 mAh g$^{-1}$) over 1000 cycles. The cycle stability of 0.02% decay per cycle at 0.9 mg cm$^{-2}$ loading is among the best cycling

performances of Si anodes reported to date. Most of the high cycling stability of Si anodes is achieved only at a low materials loading. However, a high areal loading with a long cycle life is required for commercialization of Si anodes. We therefore investigated the cycling stability of Si@C at a high loading from 1.0 to 1.9 mg $cm^{-2}$. At 1.0 mg $cm^{-2}$ loading, the Si@C anodes can provide 1.7 mAh $cm^{-2}$ (1700 mAh $g^{-1}$) reversible capacity, with a first Coulombic efficiency of 87% at 100 mA $g^{-1}$ current. At 1000 mA $g^{-1}$, no obvious capacity decay is observed from the 4th to 700th cycle. Even at 1.9 mg $cm^{-2}$ loading with an areal capacity of 2.7 mAh $cm^{-2}$ at 100 mA $g^{-1}$ (Figure 4d), which is similar to the capacity in a commercial lithium-ion battery anodes, a stable capacity of 300 mAh $g^{-1}$ at 1000 mA $g^{-1}$ for over 400 cycles is achieved. At slightly low mass loadings of 1.5 and 1.7 mg $cm^{-2}$, the 480 mAh $g^{-1}$ for over 500 stable cycles and the 400 mAh $g^{-1}$ for over 400 cycles are also achieved, respectively. To the best of our knowledge, high capacity and stable cycling at such a high mass loading level have rarely been reported for silicon anodes.

The Si@C anodes with 0.9 mg $cm^{-2}$ loading also demonstrate a very good rate performance. Figure 4e shows Coulombic efficiency and rate performance of Si@C composite anode at different current densities, from 100 to 4000 $mAg^{-1}$. Again, a high first-cycle Coulombic efficiency of 87% is reached at 100 mA $g^{-1}$, and then jumps to 96% in the second cycle and reaches near 99.7% after the fifth cycle. The Si@C anode delivers a stable capacity of 2000 mAh $g^{-1}$ at 100 mA $g^{-1}$, 1600 mAh $g^{-1}$ at 250 mA $g^{-1}$, 800 mAh $g^{-1}$ at 1000 mA $g^{-1}$, and 420 mAh $g^{-1}$ at 4000 mA $g^{-1}$. When the current reduces back to 250 $mAg^{-1}$, the capacity returns to 1600 mAh $g^{-1}$. A further increase in the current to 2000 mA $g^{-1}$ causes the capacity to reach its original value of 600 mAh $g^{-1}$. The high rate performance and cycling stability of Si@C may be attributed to the small and stable reaction resistances. Electrochemical impedance spectra (EIS) were used to compare the reaction resistance of Si and Si@C at different charge/discharge cycles. Figure S8 in Supporting Information shows the impedance of fully delithiated Si@C and Si anodes at the 1st, 20th, and 40th cycles. The EIS spectra show a depressed semicircle in the high frequency and a line in the low frequency. The high-frequency depressed semicircle is attributed to the interface impedance, including SEI film and charge transfer, and the low-frequency line is due to Li-ion diffusion in the Si anodes.[42,43] The interface impedance of Si gradually increases with charge/discharge cycles, but the Si@C remains stable over the 40th cycle. The increased interface impedance of Si is attributed to the lose contact between Si and carbon due to the volume change of Si, increasing the charge transfer resistance. Although the defect-abundant Si nanorods are structurally stable as demonstrated by a stable capacity over 200 cycles in Figure 4c, maintaining

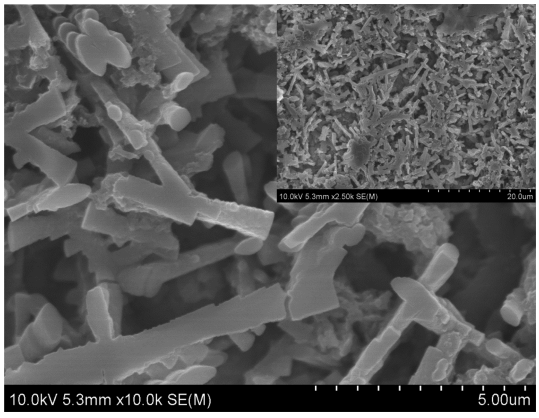


**Figure 5. SEM images of quenched Si nanorods with modifier after 200 charge/discharge cycles at 300 mA $g^{-1}$. The electrode was soaked in DMC solution for 12 h, and then washed with water for several times. The sodium alginate binder and carbon black and graphite, and Si were washed out.**

the electronic conduction of Si anodes still remains critical for the high performance electrode. Uniquely, the carbon-derived from self-polymerized polydopamine (PDA) can strongly anchor to Si nanorods (Supporting Information Figure S6 and Figure 4d), which not only improves electronic conduction but also effectively accommodates the volume change of Si and maintains the low interface resistance. The EIS of Si@C anodes in Supporting Information Figure S8 confirms the stable interface impedance of over 40 cycles due to a stable structure and good electrical contact in cycling process.

The structural stability of Si@C nanorods during charge/discharge cycles was further confirmed by the postanalysis of the electrode using SEM. As shown in Figure 5, Si@C nanorods at 1.0 mg $cm^{-2}$ still maintain original morphology after 200 charge/discharge cycles. It is well-known that Si nanowire/nanorod will become a porous structure after many charge/discharge cycles due to the opening and closing of cracks, and electrochemical welding in the lithiation/delithiation cycles,[33,44] where the anisotropy lithiation intensifies the crack formation. However, no pores and cracks are observed in the defect-abundant Si nanorods even after 200 deep charge/discharge cycles, suggesting the pre-existing defects play an important role in stabilizing the structure.

The excellent electrochemical performance of Si@C composite anodes is attributed to the unique structure of Si nanorods. The small surface area and formation of artificial surface $Al_2O_3$ and $SiO_x$ SEI (Supporting Information Figure S1g), due to Al doping in Si, significantly increases the first-cycle Coulombic efficiency to above 87−90%; meanwhile, the conformal and dense carbon coating derived from the self-polymerized PDA strongly anchoring to Si (Supporting Information Figure S6, Figure 3d) can maintain the high first-cycle Coulombic efficiency of >84% and electronic conduction of the Si anodes during the charge/discharge

cycles, thus enhancing the cycle stability. Moreover, the large number of defects in Si nanorods generated through isotropy "out-of-plane growth" may result in isotropic lithiation and promote uniform plastic deformation through pre-existing defects to relax the stress, thus enhancing the cycling stability.

## CONCLUSIONS

In summary, Al/Na doped and defect abundant Si nanorods (200 nm × 5−20 $\mu$m) with low surface area (13 $m^2 g^{-1}$) were successfully obtained by simply etching the refined eutectic Al−13% Si ingots. The refined eutectic Al−13% Si alloys were casted under ultrafast solidification after adding modifiers into the melting Al−Si alloy, in which massive defects (twins, stacking faults, dislocations) are generated and Al and Na are doped in the eutectic Si, resulting in isotropy "out-of-plane growth". The refined eutectic Si nanorods show 87−90% of the first Coulombic efficiency due to low surface area and formation of $Al_2O_3$ artificial SEI on Si surface, and maintain a capacity of ~600 mAh $g^{-1}$ at 300 mA $g^{-1}$ for over 200 cycles. The electrochemical performance of Si nanorods was further enhanced by coating a dense carbon layer (~10 nm) on Si nanorods through the carbonization of polydopamine (PDA) films (with 60% carbonization yield) on Si surfaces. The Si@C nanorods still maintained high first-cycle Coulombic efficiency of >84%, and a high capacity of 2000 mAh $g^{-1}$ was achieved at 100 mA $g^{-1}$ and maintained 700 mAh $g^{-1}$ at 1000 mA $g^{-1}$ current for over 1000 cycles. Even at a high loading of 1.9 mg $cm^{-2}$ (corresponding areal capacity of 2.7 mAh $cm^{-2}$ at 100 mA $g^{-1}$), the Si@C anodes still stably cycle at 1000 mA $g^{-1}$ over 400 cycles, which is among the best performance reported to date. In addition, the low-cost refined eutectic Al−Si alloys through rapid solidification and modification have been widely used in foundry industry for large-scale production of high tensile elongation materials. However, this cheap and highly elongated eutectic Si has never been tested in Li-ion batteries. The high-performance Si@C nanorods synthesized by simply etching the low-cost refined Al−Si alloys and polymer carbonization provide the opportunity to commercialize Si anodes in Li-ion batteries.

## EXPERIMENTAL SECTION

**Electrode Preparation.** The schematics synthesis process of Si@C is shown in Figure 1. The eutectic Al−13% Si ingots were first fabricated by melting Al−10% Si and Al−20% Si intermediate alloys (Jiangsu Hualv Co., China) in an induction furnace at 760 °C and then casting into water circulated copper molds after adding 3% Na salt modifiers (Jiangsu Hualv Co., China). The eutectic Al−13% Si ingot was cut into small chips and then placed into an 8% HCl (AR) stirring solution to remove Al. Si nanorods were then obtained after repeat filtering and washing using deionized water and then dried in a vacuum at 80 °C.

Carbon-coated Si nanorods were constructed by self-polymerization of dopamine (DA) into PDA on Si surfaces, and then carbonization at 800 °C. First, 0.5 g of Si powders was added into the 10 mM Tris-buffer solution (200 mL, pH 8.5). After ultrasonical dispersion for 30 min, 0.5 g of DA was added into the solution and then the solution was ultrasonically dispersed again for 20 min. After that, the mixture solution was self-polymerized in aerobic condition for 24 h. The resultant mixture was filtered and washed with deionized water for several times, and then dried at 70 °C under a vacuum to obtain a Si@PDA composite. Finally, the Si@C was obtained after carbonization of Si@PDA under argon protection at 800 °C for 2 h with a heating rate of 5 °C/min. For comparison, Si/C composite (PVDF-derived carbon) was also prepared using a similar procedure to the above, and used as a control sample to evaluate the bonding between Si and C. The actual carbon content in the Si@C composites was measured using thermogravimetric analysis (TGA) on a Netzsch STA409PC (Germany) with a heating rate of 10 °C/min, and air as the purge gas. Nitrogen sorption isotherms were conducted using a 3H-2000PS2 analysis station (Beishide instrument Co. China) automated gas sorption system at −196 °C. Specific surface areas and pore size distributions were calculated using the Brunauer−Emmett−Teller theory and the Barrett−Joyner−Halenda method. Specific pore volumes were measured at a relative pressure of 0.99.

**Structural Cauterization.** X-ray diffraction (XRD) patterns of samples were recorded in the 2-$\theta$ range from 10° to 80° using a D8 Advance X-ray diffractometer (Japan) with Cu K$\alpha$ radiation. The Raman spectrum was collected from 400 to 2000 $cm^{-1}$ on an Acton Spectra Pro 2500i Raman Spectrometer using the 532 nm excited wave of an Ar ion laser operated at 10 mW. Fourier transform infrared (FTIR) spectra were recorded on a NICOLEF-5DX spectrometer in the frequency range of 4000−400 $cm^{-1}$. Scanning electron microscope (SEM) images equipped with an energy dispersive X-ray spectrometry (EDS) were used to characterize the Si based composites using a S4800 (Japan). The transmission electron microscopy (TEM) samples were examined in a Tecnai G2 F20 microscope. High-resolution imaging and microanalysis were performed with an FEI Titan 80-300 analytical scanning transmission electron microscope (STEM) operated at 300 kV accelerating voltage.

**Electrochemical Measurements.** Si electrodes were prepared by mixing Si (carbon coated Si nanorods (Si@C), Si nanorods (Si), or PVDF-derived carbon coated Si nanorods (Si/C) with graphite, super P carbon black, and sodium alginate at the ratio of 56% Si, 14% graphite, 15% carbon, and 15% binder. Both Si and graphite are considered as active materials, and the specific capacity is calculated based on the total weight of Si and graphite (80 Si/20 G), which is 70% of total electrode weight. Other 30% weight is carbon black and binder. Distilled water was added into the mixture to form a slurry, which is then pasted on a copper foil with active material (80 Si/20 G) loading from 0.9 to 1.9 mg $cm^{-2}$. After a drying step in a vacuum oven at 100 °C overnight, the electrodes were assembled in coin cells in a dry argon glovebox (SG1200/750TS, Vigor) with Li metal as the counter and the reference electrode. The electrolyte was 1 M $LiPF_6$ in a mixture of EC (ethylenecarbonate), DEC (diethyl carbonate), and DMC (dimethyl carbonate) in a 1:1:1 volume ratio with 15 wt % fluorinated ethylene carbonate (FEC) as an additive. A microporous membrane (Celgard 2400) was used as the separator. All the cells were tested using galvanostatic charge−discharge protocols on a Land CT2001A Battery Testing System (Land Instruments) at room temperature. The anodes were charged/discharged in the voltage range of 0.01−1.5 V at a current density of 1000 mA $g^{-1}$ for long-term cycling stability test after first two cycles at 100 mA $g^{-1}$ for activation. The area-specific-capacity was calculated based on the capacity of Si/C at 100 mA/g. Electrochemical impedance spectra (EIS) were measured in the frequency ranges from 100 kHz to 10 mHz on a PARSTAT 4000 workstation (PARSTAT Co., U.S.A.)

*Conflict of Interest:* The authors declare no competing financial interest.

*Supporting Information Available:* XRD patterns and SEM images; TEM image and SAED patterns of eutectic Si from quenched and modified Al−13% Si alloy; morphologies of Si from Al−13% Si ignot; TG analysis of the carbon coated Si nanorods; Raman scattering spectra and FTIR spectra of the Si nanorods and carbon coated Si nanorods; $N_2$ adsorption/desorption isotherms of Si and Si@C; EIS of Si@C. The Supporting Information is available free of charge on the ACS Publications website at DOI: 10.1021/acsnano.5b02565.

*Acknowledgment.* We acknowledge the support of the National Natural Science Foundation of China (Grant no. 31100687), Heilongjiang Province Science and Technology Innovation Team (Grant no.2012TD010) and the Principal Fund Project of Jiamusi University (No.xzyf2013-05). The SEM and TEM test were supported by Nanostructures for Electrical Energy Storage (NEES), an Energy Frontier Research Center funded by the U.S. Department of Energy, Office of Science, Office of Basic Energy Sciences under Award No. DESC0001160.

## REFERENCES AND NOTES

1. Armand, M.; Tarascon, J. M. Building Better Batteries. *Nature* **2008**, *451*, 652–657.
2. Li, X. L.; Gu, M.; Hu, S. Y.; Kennard, R.; Yan, P. F.; Chen, X. L.; Wang, C. M.; Sailor, M. J.; Zhang, J. G.; Liu, J. Mesoporous Silicon Sponge as an Anti-Pulverization Structure for High-Performance Lithium-Ion Battery Anodes. *Nat. Commun.* **2015**No. 410510.1038/ncomms5105.
3. Zhang, H. P.; Fu, L. J.; Wu, Y. P.; Wu, H. Q.; Takamura, T. Research Progress in Anode Materials for Li Ion Batteries. *Battery* **2005**, *35*, 274–275.
4. Cao, G. S.; Zhao, X. B.; Li, T.; Lu, C. P. $Zn_4Sb_3$(−C7) Powders as a Potential Anode for Lithium-Ion Batteries. *J. Power Sources* **2001**, *94*, 102–107.
5. Boukamp, B. A.; Lesh, G. C.; Huggins, R. A. All-Solid Lithium Electrodes with Mixed Conductor Matrix. *J. Electrochem. Soc.* **1981**, *128*, 725–729.
6. Megahed, S.; Scrosati, B. Lithium-Ion Rechargeable Batteries. *J. Power Sources* **1994**, *51*, 79–101.
7. Ryu, J. H.; Kim, J. W.; Sung, Y. E.; Oh, S. M. Failure Modes of Silicon Powder Negative Electrode in Lithium Secondary Batteries. *Electrochem. Solid State Lett.* **2004**, *7*, A306–A309.
8. Ha, J.; Paik, U. Hydrogen Treated, Cap-opened Si Nanotubes Array Anode for High Power Lithium Ion Battery. *J. Power Sources* **2013**, *244*, 463–468.
9. Kim, H.; Seo, M.; Park, M. H.; Chen, X. F.; Huang, Y.; Chen, J. J.; Chao, L.; Zhang, X.; Huang, H. J. Preparation of Graphene Supported Porous Si@C Ternary Composites and Their Electrochemical Performance as High Capacity Anode Materials for Li-Ion Batteries. *Angew. Chem., Int. Ed.* **2010**, *49*, 2146–2149.
10. Du, F. H.; Li, B.; Fu, W.; Xiong, Y. J.; Wang, K. X.; Chen, J. S. Surface Binding of Polypyrrole on Porous Silicon Hollow Nanospheres for Li-Ion Battery Anodes with High Structure Stability. *Adv. Mater.* **2014**, *26*, 6145–6150.
11. Lee, B. S.; Son, S. B.; Park, K. M.; Seo, J. H.; Lee, S. H.; Choi, I. S.; Oh, K. H.; Yu, W. R. Fabrication of Si Core/C Shell Nanofibers and Their Electrochemical Performances as a Lithium-Ion Battery Anode. *J. Power Sources* **2012**, *206*, 267–273.
12. Liu, N.; Lu, Z. D.; Zhao, J.; Matthew, T. M.; Lee, H. W.; Zhao, W. T.; Cui, Y. A Pomegranate-Inspired Nanoscale Design for Large-Volume Change Lithium Battery Anodes. *Nat. Nanotechnol.* **2014**, *9*, 187–192.
13. Yi, R.; Dai, F.; Gordin, M. L.; Chen, S.; Wang, D. Micro-sized Si-C Composite with Interconnected Nanoscale Building Blocks as High-Performance Anodes for Practical Application in Lithium-Ion Batteries. *Adv. Energy Mater.* **2013**, *3*, 295–300.
14. Favors, Z.; Wang, W.; Bay, H. H.; Mutlu1, Z.; Ahmed, K.; Liu, C.; Ozkan, M.; Ozkan, C. S.; Ozkan, M. Scalable Synthesis of Nano-Silicon from Beach Sand for Long Cycle Life Li-Ion Batteries. *Sci. Rep.* **2014**, *4*, 5623–5629.
15. McSweeney, W.; Geaney, H.; Colm; O'Dwyer, C. Metal Assisted Chemical Etching of Silicon and the Behavior of Nanoscale Silicon Materials as Li-Ion Battery Anodes. *Nano Res.* **2015**, *8*, 1395–1442.
16. Liu, X. H.; Zheng, H.; Zhong, L.; Huang, S.; Karki, K.; Zhang, L. Q.; Liu, Y.; Kushima, A.; Liang, W. T.; Wang, J. W.; et al. Anisotropic Swelling and Fracture of Silicon Nanowires during Lithiation. *Nano Lett.* **2011**, *11*, 3312–3318.
17. Liu, X. H.; Huang, S.; Picraux, S. T.; Li, J.; Zhu, T.; Huang, J. Y. Reversible Nanopore Formation in Ge Nanowires during Lithiation-Delithiation Cycling: An *in Situ* TEM Study. *Nano Lett.* **2011**, *11*, 3991–3997.
18. Soni, S. K.; Sheldon, B. W.; Xiao, X.; Tokranov, A. Thickness Effects on the Lithiation of Amorphous Silicon Thin Films. *Scr. Mater.* **2011**, *64*, 307–310.
19. Sethuraman, V. A.; Chon, M. J.; Shimshak, M.; Srinivasan, V.; Guduru, P. R. In Situ Measurements of Stress Evolution in Silicon Thin Films during Electrochemical Lithiation and Delithiation. *J. Power Sources* **2010**, *195*, 5062–5066.
20. Sethuraman, V. A.; Srinivasan, V.; Bower, A. F.; Guduru, P. R. *In Situ* Measurements of Stress-Potential Coupling in Lithiated Silicon. *J. Electrochem. Soc.* **2010**, *157*, A1253–1261.
21. Goldman, J. L.; Long, B. R.; Gewirth, A. A.; Nuzzo, R. G. Strain Anisotropies and Self-Limiting Capacities in Single-Crystalline 3D Silicon Microstructures: Models for High Energy Density Lithium-Ion Battery Anodes. *Adv. Funct. Mater.* **2011**, *21*, 2412–2422.
22. Sheldon, B. W.; Soni, S. K.; Xiao, X.; Que, Y. Stress Contributions to Solution Thermodynamics in Li−Si Alloys. *Electrochem. Solid State Lett.* **2012**, *15*, A9.
23. Hwang, G.; Park, H.; Bok, T.; Choi, S.; Lee, S.; Hwang, I.; Choi, N.; Seo, K.; Park, S. A High-Performance Nanoporous Si/Al2O3 Foam Lithium-Ion Battery Anode Fabricated by Selective Chemical Etching of the Al−Si Alloy and Subsequent Thermal Oxidation. *Chem. Commun.* **2015**, *51*, 4429–4432.
24. Zhou, W.; Jiang, T.; Zhou, H.; Wang, Y.; Fang, J.; Whittingham, M. S. The Nanostructure of the Si−Al Eutectic and Its Use in Lithium Batteries. *MRS Commun.* **2013**, *3*, 119–121.
25. Jiang, Z. Y.; Li, C. L.; Hao, S. J.; Zhu, K.; Zhang, P. An Easy Way for Preparing High Performance Porous Silicon Powder by Acid Etching Al−Si Alloy Powder for Lithium Ion Battery. *Electrochim. Acta* **2014**, *115*, 393–398.
26. Dahle, A. K.; Nogita, K.; McDonald, S. D.; Dinnis, C.; Mater, L. L. Eutectic Modification and Microstructure Development in Al−Si Alloys. *Mater. Sci. Eng., A* **2005**, *413−414*, 243–248.
27. Tian, H.; Tan, X.; Xin, F.; Wang, C.; Han, W. Micro-Sized Nano-Porous Si/C Anodes for Lithium Ion Batteries. *Nano Energy* **2015**, *11*, 490–499.
28. Legrain, F.; Manzhos, S. Aluminum Doping Improves the Energetics of Lithium, Sodium, and Magnesium Storage in Silicon: A First-Principles Study. *J. Power Sources* **2015**, *274*, 65–70.
29. Kim, Y. L.; Lee, S. J.; Baik, H. K.; Lee, S. M. $Sn_2Zr_2Ag$ Alloy Thin Film Anodes. *J. Power Sources* **2003**, *119−121*, 106–109.
30. Wang, X. D.; Li, X. P.; Sun, Z. B. Research Progress of the Lithium Ion Battery Alloy Anode Materials. *Battery* **2007**, *37*, 161–163.
31. Zu, F. Q.; Li, X. Y. Functions and Mechanism of Modification Elements in Eutectic Solidification of Al-Si Alloys: A Brief Review. *China Foundry* **2014**, *11*, 287–295.
32. Hegde, S.; Prabhu, K. N. Modification of Eutectic Silicon in Al-Si Alloys. *J. Mater. Sci.* **2008**, *43*, 3009–3027.
33. Liu, X.; Liu, Y.; Kushima, A.; Zhang, S.; Zhu, T.; Li, J.; Huang, J. Y. *In Situ* TEM Experiments of Electrochemical Lithiation and Delithiation of Individual Nanostructures. *Adv. Energy Mater.* **2012**, *2*, 722–741.
34. Liu, R.; Mahurin, S. M.; Li, C.; Raymond, R. U.; Juan, C. I.; Gao, H. J.; Stephen, J. P.; Dai, S. Dopamine as a Carbon Source: The Controlled Synthesis of Hollow Carbon Spheres and Yolk-Structured Carbon Nanocomposites. *Angew. Chem., Int. Ed.* **2011**, *50*, 6799–6802.

35. Tan, Y.; Tang, Y. H.; Pei, L. Z. The Study on Raman Spectra of Si Nanowires. *Spectrosc. Spectral Anal.* **2007**, *27*, 725–729.
36. Tsu, R.; Shen, H.; Dutta, M. Correlation of Raman and Photoluminescence Spectra of Porous Silicon. *Appl. Phys. Lett.* **1992**, *60*, 112–114.
37. Julie, C. M.; Zaghib, K.; Mauger, A. Characterization of the Carbon Coating onto $LiFePO_4$ Particles Used in Lithium-Batteries. *J. Appl. Phys.* **2006**, *100*, 0635111–0635117.
38. Gao, P. F.; Fu, J. W.; Yang, J.; Lv, R. G.; Wang, J. L.; Nuli, Y. N.; Tang, X. Z. Microporous Carbon Coated Silicon Core/Shell Nanocomposite *via in Situ* Polymerization for Advanced Li-Ion Battery Anode Material. *Phys. Chem. Chem. Phys.* **2009**, *11*, 11101–11105.
39. Zhang, Y.; Xia, X.; Wang, X.; Mai, Y.; Shi, S.; Tang, Y.; Gu, C.; Tu, J. Three-Dimensional Porous Nano-Ni Supported Silicon Composite Film for High-Performance Lithium-Ion Batteries. *J. Power Sources* **2012**, *213*, 106–111.
40. Wang, M. S.; Fan, L. Z.; Huang, M.; Li, J. H.; Qu, X. H. Conversion of Diatomite to Porous Si/C Composites as Promising Anode Materials for Lithium-Ion Batteries. *J. Power Sources* **2012**, *219*, 29–35.
41. Zheng, Y.; Yang, J.; Wang, J. L.; Nuli, Y. N. Nano-Porous Si/C Composites for Anode Material ofLithium-Ion Batteries. *Electrochim. Acta* **2007**, *52*, 5863–5867.
42. Ng, S. H.; Wang, J.; Wexler, D.; Chew, S. Y.; Liu, H. K. Amorphous Carbon-Coated Silicon Nanocomposites: A Low-Temperature Synthesis *via* Spray Pyrolysis and Their Application as High-Capacity Anodes for Lithium-Ion Batteries. *J. Phys. Chem. C* **2007**, *111*, 11131–11138.
43. Shin, H. C.; Cho, W. I.; Jang, H. Electrochemical Properties of the Carbon-Coated LiFePO4 as a Cathode Material for Lithium-Ion Secondary Batteries. *J. Power Sources* **2006**, *159*, 1383–1388.
44. Chen, X.; Gerasopoulos, K.; Guo, J.; Brown, A.; Wang, C.; Ghodssi, R.; Culver, J. N. Virus-Enabled Silicon Anode for Lithium-Ion Batteries. *ACS Nano* **2010**, *4*, 5366–5372.